Systematic design of chemical oscillators. 86. Combined mechanism explaining nonlinear dynamics in bromine(III) and bromine(V) oxidations of iodide ion

Roberto De Barros Faria, Istvan Lengyel, Irving R. Epstein, and Kenneth Kustin

J. Phys. Chem., **1993**, 97 (6), 1164-1171• DOI: 10.1021/j100108a011 • Publication Date (Web): 01 May 2002

Combined Mechanism Explaining Nonlinear Dynamics in Bromine(III) and Bromine(V) Oxidations of Iodide Ion[1]

Roberto de Barros Faria,[†] István Lengyel,[‡] Irving R. Epstein,* and Kenneth Kustin*

Department of Chemistry, Brandeis University, Box 9110, Waltham, Massachusetts 02254-9110

Received: July 17, 1992; In Final Form: November 9, 1992

A mechanism is presented that explains the full range of dynamics exhibited in the oxidations of iodide ion by both bromine(III) (bromite) and bromine(V) (bromate) in closed and open reactors, including clock reactions and oscillations. This comprehensive model comprises 28 steps and 14 species, includes IBr as a reactive intermediate, and contains a reaction sequence autocatalytic in HOBr. Kinetics curves and phase diagrams simulated with this model show very good agreement with experiment. The combined model is based on a 20-step mechanism used to explain the bromine(III)-iodide clock reaction over the pH range 6-8. With additional independent species and bromine(V)-driven steps, simulations of bromine(V)-iodide oscillations in concentrated sulfuric acid are improved by this model compared with the previous model.

Introduction

The commercial availability of bromine(III) (bromite) opened up a direct approach to studying the kinetics of this strong and facile oxidant. Oscillations were soon found in the oxidation of iodide ion by bromine(III) in an open (flow) reactor, and a qualitative explanation of this nonlinear dynamical behavior was presented.[2] In parallel with this discovery, studies of the bromine(III)-I^- reaction in a closed (batch) reactor led to the discovery of a new clock reaction, for which a quantitative mechanistic explanation was provided,[3] and to a new determination of the pK_a of bromous acid ($HBrO_2$).[4]

The reaction between bromine(V) (bromate) and iodide ion in concentrated sulfuric acid exhibits clock reaction behavior in batch[5] and oscillatory behavior in flow.[6] This kinetics behavior had previously been modeled by Citri and Epstein (CE model).[7] Therefore, we decided to develop a more comprehensive, combined model, based on the Br(III)-I^- mechanism, to simulate the oxidation of I^- by both bromine(III) and bromine(V) in flow and batch reactors.

For both oxidants, essential chemical processes are similar and iodide ion is oxidized to molecular iodine; in excess oxidant, molecular iodine is further transformed to iodine(V). If the oxidant is bromine(III), nonlinear dynamics are observed from pH 6 to pH 8, because this reagent is very reactive and does not require as much hydrogen ion assistance as does bromine(V). Although the pK_a of $HBrO_2$ is low (3.43),[4] sufficient $HBrO_2$ is present to initiate clock reaction and oscillatory behavior in less than acidic media. Clock behavior was observed. in buffered solutions at pH 6-8. As the pH becomes more acidic, reaction rates increase, and experimental observation becomes more difficult.

If the oxidant is bromine(V), very acid conditions are the rule, because of the oxidant's lower reactivity. Sulfur acid of concentration 0.04 M was used to produce clock reaction behavior in a closed reactor, and 1.5 M sulfuric acid was used to induce oscillations in an open reactor. Since the first intermediate formed from bromine(V) when oxidizing iodide should be bromine(III), the bromine(III)-iodide mechanism should be a subset of the bromine(V)-iodide mechanism. The acids $HBrO_2$ and HOBr generated by the overall reaction are sufficiently weak that in concentrated sulfuric acid their dissociation behavior need not be considered.

Methods

The calculations were performed on a 386/33 MHz PC-compatible microcomputer using a program written by one of us (I.L.) in Turbo Pascal to solve autonomous ordinary differential equation systems by a semiimplicit Runge-Kutta method.[8]

Bromine(III)-Iodide. The 20-step, 12-species mechanism used to model the batch reactions of this system[3] forms the basis of the combined model (Table I). Reaction R9 as written emphasizes the fact that its velocity depends only on the concentrations of HIO_2 and I^-. Each mole of this reaction produces 2 mol of HOI and consumes 1 mol each of HIO_2, I^-, and H^+; IO^- is not considered an independent species. To speed up calculations when treating the bromine(III)-I^- system, the steps associated with reactions R17-R20, dealing exclusively with Br(V), which is not a reagent in this system, and reactions R4, R5, and the reverse of reaction R11 and R14 were eliminated, because they contribute to the rate only in highly acidic conditions. Reintroduction of these reactions into the mechanism had no significant effect on the results of the simulation. The batch reactions were buffered, and $[H^+]$ was held constant; the flow reactions were not buffered, and $[H^+]$ was allowed to vary in simulating oscillations in flow reactors.

Bromine(V)-Iodide. Some economies in the model are feasible when treating dynamical behavior initiated by bromine(V) acting as reagent. Reactions R1 and R8 (Table I) could be eliminated, since no significant amounts of BrO_2^- or BrO^- are expected at $[H^+] \approx 1$ M. In addition, since the sulfuric acid concentration is much higher than the concentrations of all other reagents, reaction R21 can be eliminated and $[H^+]$ held constant during all calculations. Hydroxide ion concentration was calculated from an apparent, ionic strength-dependent K_w at $\mu = 1.5$ M for flow simulations and $\mu = 0.05$ M for batch simulations.[9]

Rate Constant Selection. Because the combined mechanism (Table I) is an expanded version of the mechanism used to model batch results in the system bromine(III)-iodide,[3] comments are restricted to reactions pertaining to bromine(V)-iodide.

R4: Our value is essentially the same as that of a recently proposed model which successfully simulates chaos in the Belousov-Zhabotinskii (BZ) reaction.[10,11] It is well within the range ($(1-4) \times 10^6$ M^{-2} s^{-1}) determined experimentally by following the disproportionation of $HBrO_2$ with a bromide ion selective electrode interpreted by corrosion potential theory.[12]

R5: We use the experimentally determined value at 24 °C and $[H_2SO_4] = 0.5$ M.[13]

R17: We use the CE model value, based on experimental studies of this reaction at 25 °C and $\mu = 0.2$ M.[7]

[†] Departamento de Química Inorgânica, Instituto de Química, Universidade Federal do Rio de Janeiro, 21941 Rio de Janeiro, RJ, Brazil.

[‡] Institute of Physical Chemistry, Kossuth Lajos University, Debrecen, H-4010 Hungary.

0022-3654/93/2097-1164$04.00/0

TABLE I: Reaction Mechanism, Forward and Reverse Rate Constants

no.		forward rate const	reverse rate const
	$HBrO_2$ Reactions		
R1	$HBrO_2 \rightleftarrows BrO_2^- + H^+$	3.73×10^6 s^{-1}	1×10^{10} M^{-1} s^{-1}
R2	$HBrO_2 + I^- \rightarrow HOI + BrO^-$	7.46×10^5 M^{-1} s^{-1}	
R3	$HBrO_2 + HOI \rightarrow HOBr + HIO_2$	6×10^7 M^{-1} s^{-1}	
R4	$HBrO_2 + Br^- + H^+ \rightarrow 2HOBr$	2×10^6 M^{-2} s^{-1}	
R5	$2HBrO_2 \rightarrow HOBr + BrO_3^- + H^+$	2.2×10^3 M^{-1} s^{-1}	
	Some HOBr Reactions		
R6	$HOBr + HOI \rightarrow Br^- + HIO_2 + H^+$	1×10^6 M^{-1} s^{-1}	
R7	$HOBr + HIO_2 \rightarrow Br^- + IO_3^- + 2H^+$	1×10^6 M^{-1} s^{-1}	
R8	$HOBr \rightleftarrows H^+ + BrO^-$	15.8 s^{-1}	1×10^{10} M^{-1} s^{-1}
	Some HIO_2 Reactions		
R9	$HIO_2 + I^- \rightarrow HOI + IO^- (\rightarrow HOI)$	2×10^5 M^{-1} s^{-1}	
R10	$HIO_2 + HOI \rightarrow IO_3^- + I^- + 2H^+$	6×10^3 M^{-1} s^{-1}	
	IBr Reactions		
R11	$IBr + H_2O \rightarrow Br^- + HOI + H^+$	8×10^5 s^{-1}	4.1×10^{12} M^{-2} s^{-1}
R12	$HOBr + I^- \rightarrow IBr + OH^-$	5×10^9 M^{-1} s^{-1}	
R13	$HOBr + I_2 \rightarrow IBr + HOI$	1×10^7 M^{-1} s^{-1}	
R14	$IBr + I^- \rightarrow I_2 + Br^-$	2×10^9 M^{-1} s^{-1}	4.74×10^3 M^{-1} s^{-1}
	Iodine Hydrolysis		
R15	$I_2 + OH^- \rightleftarrows I_2OH^-$	1×10^{10} M^{-1} s^{-1}	6×10^5 s^{-1}
R16	$I_2OH^- \rightleftarrows HOI + I^-$	6×10^3 s^{-1}	2.5×10^6 M^{-1} s^{-1}
	BrO_3^- Reactions		
R17	$BrO_3^- + I^- + 2H^+ \rightarrow HBrO_2 + HOI$	45 M^{-3} s^{-1}	
R18	$BrO_3^- + HOI + H^+ \rightarrow HBrO_2 + HIO_2$	8×10^3 M^{-2} s^{-1}	
R19	$BrO_3^- + HIO_2 \rightarrow HBrO_2 + IO_3^-$	10 M^{-1} s^{-1}	
R20	$BrO_3^- + Br^- + 2H^+ \rightarrow HBrO_2 + HOBr$	2 M^{-3} s^{-1}	
	Water Equilibrium[a]		
R21	$H_2O \rightleftarrows H^+ + OH^-$	$(1.3 \times 10^{11})K_w$ s^{-1}	1.3×10^{11} M^{-1} s^{-1}

[a] For each different ionic strength K_w was calculated using the formulas in ref 9.

R18: Values previously used for this reaction were 1.5×10^2 and 8×10^2 M^{-2} s^{-1}.[7,14] For our model, the best fit requires an order of magnitude increase in the larger of these values.

R19: Previous values for this reaction were 1.6×10^4 and 1×10^3 M^{-1} s^{-1}.[7,14] The best value for our model is several orders of magnitude lower.

R20: Our value is the same as that used to model the BZ reaction.[10,11]

In addition to the above steps, we include the reverse of two reactions.

R11 (reverse): Our value is based on the experimentally measured forward rate constant[15] and the thermodynamic equilibrium constant calculated from the free energy of formation of the components of this reaction.[16] If this value were based on the experimentally measured equilibrium constant,[15] 2.4×10^{-7} M^2 at 25 °C and $\mu = 0.5$ M, the value of the reverse rate constant would be 3.3×10^{12} M^{-2} s^{-1}, which is slightly less than the value we used. Using the lower value moves the oscillation region to values of the input flow rate, k_0 (s^{-1}), higher than observed. After accounting for the activity coefficients of Br^- and H^+, we calculate a value of 4.4×10^{12} M^{-2} s^{-1} at $\mu = 1$ M that is quite close to the value we used.[17,18]

R14 (reverse): Our value is based on the experimental rate constant[15] for formation of I_2Br^- and the thermodynamic equilibrium constant calculated from the free energy of formation of the components of reaction R14.[16]

Particular attention was paid to the bromine hydrolysis equilibrium (1). This reaction was included at first in our model

$$HOBr + Br^- + H^+ \rightleftarrows Br_2 + H_2O \qquad (1)$$

with the rate constants used successfully in modeling the BZ reaction,[10,11] which entails use of an apparent equilibrium constant of 1.15×10^9 M^{-2}. A value of 1.5×10^9 M^{-2} has also been proposed for this constant, based on experimental results at 20 °C for the disproportionation of HOBr in 1 M H_2SO_4.[19] Used in our model, these values remove oscillations from reaction mixtures where they normally occur; for example, $[BrO_3^-]_0 = 5 \times 10^{-3}$ M, $[I^-]_0 = 2.5 \times 10^{-3}$ M, $[H^+]_0 = 1.5$ M. A value of 7×10^7 M^2 was selected for this equilibrium constant, in an experimental study at 20 °C and 1 M H_2SO_4, to decide if bromine or bromide is the control intermediate in the BZ oscillating reaction.[20] Unpublished experimental results (collected by H. J. Lamberz) in 1 M H_2SO_4 were cited,[20] which confirmed a lower value for this equilibrium constant. Use of the lower equilibrium constant restores oscillations to our modeling studies. Activity coefficients calculated with the Davies formula[18] for Br^-, and with the Capone et al. formula[17] for H^+, were used to calculate an equilibrium constant of 2.2×10^8 M^{-2} at $\mu = 1.0$ M from the experimental equilibrium constant measured at 20 °C and $\mu = 0.1$ M by the temperature-jump relaxation technique.[21] Therefore, the difference in ionic strength does not justify use of a value roughly 10 times higher. In addition, we calculate for this reaction, from ΔH_f° of its reactants and products,[16] $\Delta H^\circ = -52.2$ kJ mol^{-1}. Thus, the value of the equilibrium constant at 25 °C can be calculated with use of the van't Hoff equation, which leads to the value 1.5×10^8 M^{-2}.[22] From an a posteriori consideration of the results of our calculations, we noted that, with this lower equilibrium constant value, inclusion of this reaction does not affect the calculations. We therefore eliminated bromine hydrolysis and reduced the complexity of the model by one species and two reactions.

Results

Bromine(III)–Iodide. Since the bromine(III)–I^- mechanism has yielded excellent simulations of the batch reactions, we emphasize oscillations. Straightforward comparison between experiment and simulation is difficult, because the shapes of the oscillations are sensitive to stirring frequency, becoming more complex at higher frequencies.[2] To facilitate comparisons, we use the same aspect ratios and concentrations in our figures as in the earlier reports. Both the relatively simple shapes of pH oscillations (Figure 1a) and the more complex shape of $[I^-]$ oscillations (Figure 1b) are closely simulated, bearing the greatest resemblance to experimental results at high stirring frequency.

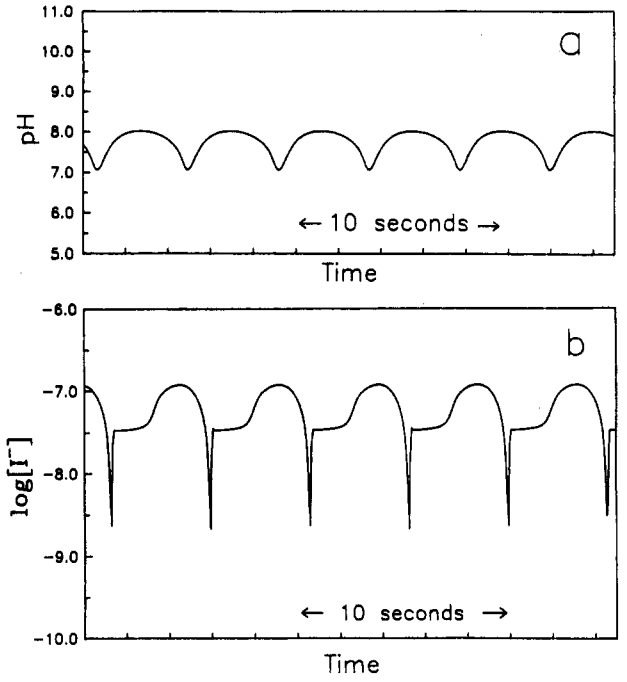

Figure 1. Br(III)–I⁻: oscillations in pH (a) and log [I⁻] (b). (a) Fixed constraints: $[BrO_2^-]_0 = 1.94 \times 10^{-3}$ M, $[I^-]_0 = 8 \times 10^{-4}$ M, $[H^+]_0 = 1 \times 10^{-4}$ M, $k_0 = 3 \times 10^{-3}$ s^{-1}. (b) Fixed constraints: $[BrO_2^-]_0 = 2 \times 10^{-3}$ M, $[I^-]_0 = 1 \times 10^{-3}$ M, $[H^+]_0 = 1 \times 10^{-4}$ M, $k_0 = 3 \times 10^{-3}$ s^{-1}.

TABLE II: Oscillation Regions for the System Bromine(II)–Iodide

$[I^-]_0$ (M)	$[BrO_2^-]_0$ (M)	$[H^+]_0$ (M)	k_0 (s^{-1})
9×10^{-4} to 1.3×10^{-3}	2×10^{-3}	1×10^{-4}	3×10^{-3}
1×10^{-3}	1.5×10^{-3} to 2.4×10^{-3}	1×10^{-4}	3×10^{-3}
1×10^{-3}	2×10^{-3}	6×10^{-5} to 1.6×10^{-4}	3×10^{-3}
1×10^{-3}	2×10^{-3}	1×10^{-4}	1.6×10^{-3} to 1.3×10^{-2}

The simulated period of 4.8 s is shorter than the experimental period of 75 s; this disparity is analyzed in the Discussion section.

Several ranges of oscillation are found in experiment and simulation (Table II). For comparison, the experimental ranges for oscillation are as follows:[2]

$$[BrO_2^-]_0/[I^-]_0 = 2.0 \pm 0.2$$

$$[I^-]_0 = 2.5 \times 10^{-4} \text{ to } 2 \times 10^{-3} \text{M}$$

$$[BrO_2^-]_0 = 5 \times 10^{-4} \text{ to } 4 \times 10^{-3} \text{ M}$$

$$k_0 = 3 \times 10^{-3} \text{ to } 1.5 \times 10^{-2} \text{ s}^{-1}$$

where $[I^-]_0$ and $[BrO_2^-]_0$ are inflow concentrations. The experimental inflow concentrations of Figure 1, $[I^-]_0 = 1 \times 10^{-3}$ M, $[BrO_2^-]_0 = 2 \times 10^{-3}$ M, lie well within the calculated oscillation region. Experimental and simulation ranges overlap quite well, but the experimental range is somewhat broader than the simulated range for each constraint in Table II.

Consider, next, a phase diagram (Figure 2) calculated for this system using inflow concentrations of iodide and bromine(III) as parameters. (To check the accuracy of some of the phase portraits, we used the program Phaseplane.[23] Within the accuracy of the calculation, agreement was perfect.) As the diagram indicates, the simulation reveals the existence of three different steady states (Table III), two of them, SSI and SSII, reported experimentally.

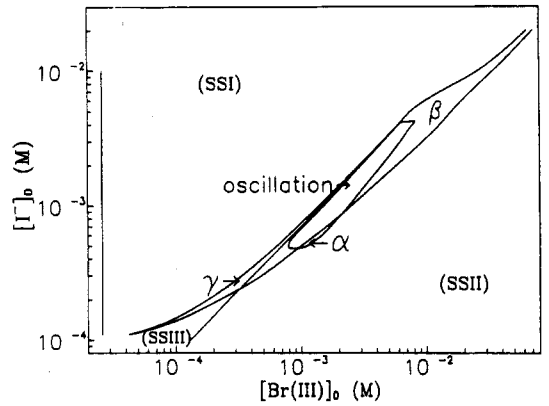

Figure 2. Br(III)–I⁻: phase diagram. Fixed constraints: $k_0 = 3 \times 10^{-3}$ s^{-1}, $[H^+]_0 = 1 \times 10^{-4}$ M.

TABLE III: Steady States for the Bromine(III)–Iodide System

	pH	$[I^-]$
SSI	high	high
SSII	low	low
SSIII	lowest	intermediate

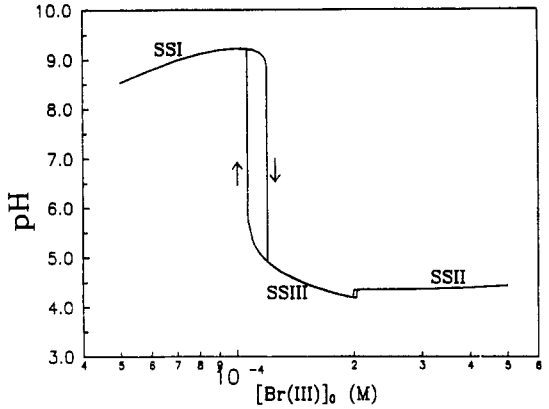

Figure 3. Br(III)–I⁻: pH–[Br(III)] phase plane. Fixed constraints: $[I^-]_0 = 1.5 \times 10^{-4}$ M, $[H^+]_0 = 1.0 \times 10^{-4}$ M, $k_0 = 3.0 \times 10^{-3}$ s^{-1}.

To see how the additional steady state, SSIII, affects the behavior of the system, we examine changes in pH (Figure 3), beginning with SSI at $[I^-]^0 = 1.5 \times 10^{-4}$ M, while increasing $[BrO_2^-]_0$ and keeping $[I^-]_0$ constant. Starting at 5×10^{-5} M $[BrO_2^-]_0$, the pH is 8.5 and the system is in SSI. Increasing $[BrO_2^-]_0$ causes the pH to rise, and then there is a sudden drop when SSIII is entered at $[BrO_2^-]_0 = 1.22 \times 10^{-4}$ M. Increasing $[BrO_2^-]_0$ further causes a small jump in pH that signals entry into SSII at $[BrO_2^-]_0 = 2.05 \times 10^{-4}$ M. Close to transition points, (i.e., when crossing lines on the phase diagram, Figure 2) the calculated values for pH in SSIII are lower than the values found for SSI and SSII at the same $[I^-]_0$. However, similar values of pH can be found inside SSI and SSII for other values of $[I^-]_0$. Decreasing $[BrO_2^-]_0$ does not retrace the same route. The transition between SSII and SSIII occurs at the same $[BrO_2^-]_0$, but the system reenters SSI at a lower $[BrO_2^-]_0$.

Oscillations can be readily attained by setting $[I^-]_0$ to such a value that increasing $[BrO_2^-]_0$ will send the system on a path that crosses region α while jumping from SSI to SSII. That is, to obtain oscillations, set, for example, $[I^-]_0 = 6 \times 10^{-4}$ M (Figure 2) and start with $[BrO_2^-]_0 = 1 \times 10^{-4}$ M. Then, increasing $[BrO_2^-]_0$ yields oscillations at $[BrO_2^-]_0 = 1.28 \times 10^{-3}$ M. Additional increase in $[BrO_2^-]_0$ causes the system to exit the oscillation region and enter SSII at $[BrO_2^-]_0 = 1.45 \times 10^{-3}$, which marks one Hopf bifurcation point (Figure 4). If $[BrO_2^-]_0$ is now decreased, the oscillation region will be entered from SSII and excited at $[BrO_2^-]_0 = 8.8 \times 10^{-4}$ M, which marks a second Hopf bifurcation point. The oscillation region is found between these

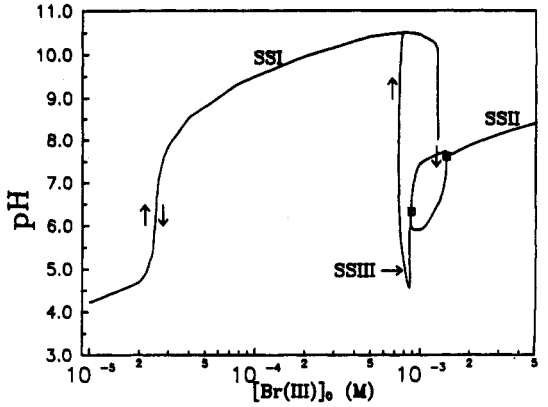

Figure 4. Br(III)–I⁻: pH–Br(III) phase plane. Fixed constraints: $[I^-]_0 = 6 \times 10^{-4}$ M, $[H^+]_0 = 1.0 \times 10^{-4}$ M, $k_0 = 3.0 \times 10^{-3}$ s^{-1}. Hopf bifurcation points are denoted by the symbol □. The closed surface encompasses the maximum and minimum pH oscillations that occur between the two Hopf bifurcation points.

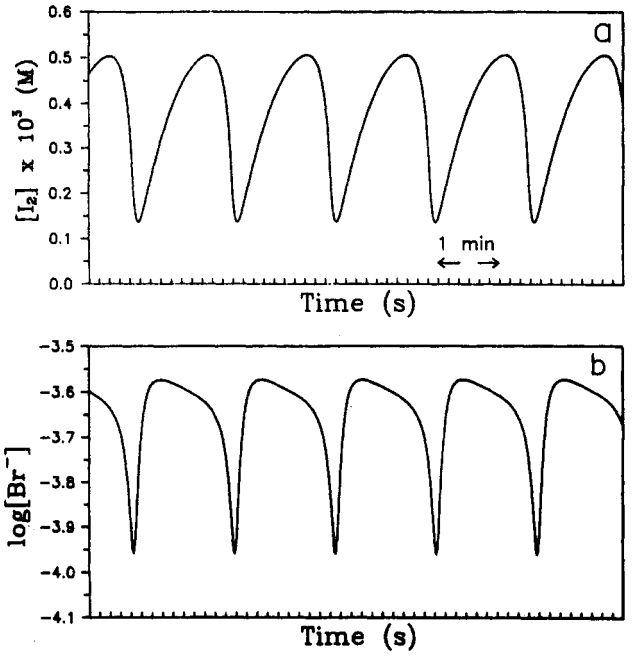

Figure 5. Br(V)–I⁻: oscillations in $[I_2]$ (a) and log $[Br^-]$ (b). Fixed constraints: $[I^-]_0 = 2.5 \times 10^{-3}$ M, $[BrO_3^-]_0 = 5.0 \times 10^{-3}$ M, $[H^+]_0 = 1.5$ M, $k_0 = 3.48 \times 10^{-2}$ s^{-1}.

two Hopf bifurcation points. In addition, at both $[BrO_2^-]_0 = 8.52 \times 10^{-4}$ and 7.88×10^{-4} M there is a decrease in pH followed by a larger increase in pH as regions β and SSI are entered, respectively. If $[I^-]_0$ is above approximately 2×10^{-3} M, no oscillation region will be found by increasing $[BrO_2^-]_0$, since SSI will jump directly to SSII, because the oscillation region is totally under the SSI branch and can be accessed only from SSII.

Regions β and γ are bistability regions shared by SSI and SSII and SSI and SSIII, respectively. The left vertical line is a limit for SSI, to the left of which nonlinear dynamics behavior is no longer displayed. This low $[BrO_2^-]_0$ limit and the region of bistability between SSIII and SSII show such a small hysteresis that they are not likely to be found experimentally and are shown as single lines on the phase diagram (Figure 2).

Bromine(V)–Iodide. Our results show some improvements when compared with the CE model.[7] The simulated batch reaction is quite similar to that observed experimentally. The times at which $[I_2]$ returns to an almost zero level are 1440 and 2100 s for $[H^+]_0 = 0.05$ and 0.04 M, respectively, which are basically the same times obtained by the CE model.[7] These times are slightly longer than the experimental values for $[H^+]_0 = 0.05$ M (1320 s) and shorter for $[H^+]_0 = 0.04$ M (4500 s).[5] The wave

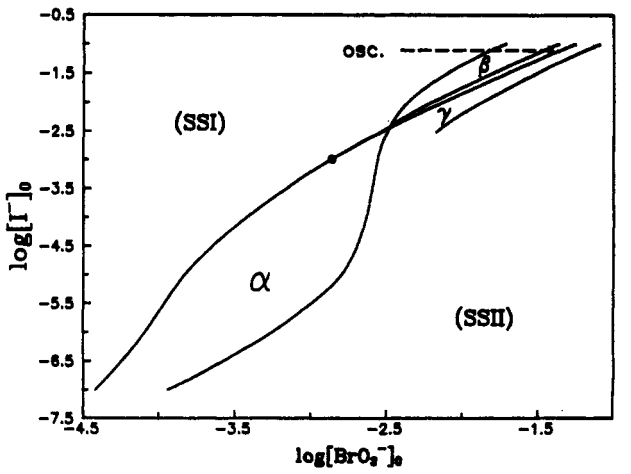

Figure 6. Br(V)–I⁻: phase diagram. The oscillation region extends from upper right to lower left until the point marked by the circle is reached. Fixed constraints: $[H^+]_0 = 1.5$ M, $k_0 = 1.2 \times 10^{-2}$ s^{-1}.

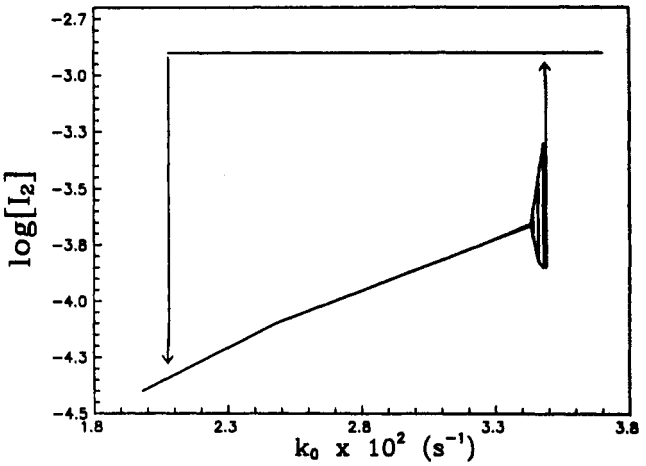

Figure 7. Br(V)–I⁻: bistability and hysteresis as a function of flow rate. Arrows indicate transition points. Fixed constraints: $[BrO_3^-]_0 = 5 \times 10^{-3}$ M, $[I^-]_0 = 2.5 \times 10^{-3}$ M, $[H^+]_0 = 1.5$ M.

form based on our model resembles experiment more closely than the CE model, especially for $[H^+]_0 = 0.04$ M.

Representative simulations of oscillations are shown in Figure 5 at conditions as close as possible to experiment.[7] The agreement with experiment in frequency, shape, and range of concentration for iodine, iodide (not shown), and bromide oscillations is excellent.

The phase diagram (Figure 6) obtained with our model is very similar to the experimental one,[6] and much better than the CE model. In our model, the oscillatory region extends down to inflow concentrations $[I^-]_0 = 1 \times 10^{-3}$ M and $[BrO_3^-]_0 = 1.4 \times 10^{-3}$ M. For $[I^-]_0 = 0.1$ M, the range of $[BrO_3^-]_0$ is 4.35×10^{-2} to 5.6×10^{-2} M. These limits are significant improvements over the CE model. The bistability region α is still too high in $[BrO_3^-]_0$ and the low end is too low in $[BrO_3^-]_0$ in contrast to the CE model, which is too high.

Bistability and hysteresis as functions of k_0 at fixed $[I^-]_0$ and $[BrO_3^-]_0$ are shown in Figure 7. The level of $[I^-]$ is similar to that of the CE model, and the oscillatory region is a bit far from experimental values. In the region of oscillation, however, we found oscillation periods of 50, 60, and 100 s for flow rates of 3.44×10^{-2}, 3.46×10^{-2}, and 3.48×10^{-2} s^{-1}, respectively, which are closer to the experimental values than are the previous values calculated with the CE model.

We found two additional transitions (Figure 6) not reported in the experimental studies. Keeping $[I^-]_0$ constant and equal to 1×10^{-2} M (Figure 6), and increasing $[BrO_3^-]_0$, starting from SSI, there occurs a decrease in $[I^-]$ at $[BrO_3^-]_0 = 4.35 \times 10^{-3}$ M, with no change in $[I_2]$, which signals entry into region β.

TABLE IV: Calculated Concentrations and Rates in SSI and SSII at Same Conditions (Bistability Region) for the System Bromine(III)–Iodide[a]

	concn (M)			concn (M)	
	SSI	SSII		SSI	SSII
$[H^+]$	1×10^{-11}	3×10^{-9}	$[HIO_2]$	6×10^{-7}	1×10^{-4}
$[I^-]$	3×10^{-5}	2×10^{-7}	[HOBr]	4×10^{-11}	1×10^{-8}
$[HBrO_2]$	1×10^{-10}	2×10^{-8}	$[I_2]$	7×10^{-7}	9×10^{-9}
[HOI]	9×10^{-4}	8×10^{-6}	[IBr]	7×10^{-12}	1×10^{-11}

	rate ($M\ s^{-1}$)			rate ($M\ s^{-1}$)	
	SSI	SSII		SSI	SSII
R2	2×10^{-9}	2×10^{-9}	R11	6×10^{-6}	8×10^{-6}
R3	6×10^{-6}	9×10^{-6}	R12	6×10^{-6}	8×10^{-6}
R6	4×10^{-8}	8×10^{-8}	R13	3×10^{-10}	9×10^{-10}
R7	2×10^{-11}	1×10^{-6}	R14	4×10^{-7}	3×10^{-9}
R9	3×10^{-6}	3×10^{-6}	R15	4×10^{-5}	3×10^{-9}
R10	3×10^{-6}	5×10^{-6}	R16	3×10^{-7}	2×10^{-9}

[a] $[I^-]_0 = 2 \times 10^{-3}$ M, $[BrO_2^-]_0 = 5 \times 10^{-3}$ M, $[H^+]_0 = 1 \times 10^{-4}$ M, $k_0 = 3 \times 10^{-3}\ s^{-1}$.

Additional increase of $[BrO_3^-]_0$ leads to encounter with and then exit from the oscillatory region. Finally, there occurs a rather sharp decrease in $[I_2]$, with no change in $[I^-]$, that signals crossing the line separating region γ from SSII. In entering region β from SSI, the change in $[I^-]$ is from 2.5×10^{-6} to 6.3×10^{-7}, which is close to the limit of most iodide-selective electrodes and can be difficult to observe experimentally. Exiting region γ to SSII changes $[I_2]$ from 1×10^{-7} to 4.0×10^{-9} M, which should be easy to observe, and which should be checked in the future. Curiously, this line could not be followed in our calculations for $[I^-]_0$ lower than 2×10^{-3} M as the changes in $[I_2]$ become smooth and not abrupt. Because of this effect, we are reluctant to designate regions β and γ as separate steady states.

Discussion

Bromine(III)–Iodide. In this system, oscillatory behavior entails alternation between two pseudo steady states resembling SSI and SSII. All reactions proceed with lower speed in SSI than in SSII, as found experimentaly, except for reactions R14–R16 (Table IV). State SSI is characterized by higher $[I^-]$, [HOI], and pH than SSII. The most important reactions are reactions R3, R12, R11, and R9, which sum to

$$HBrO_2 + 2I^- + H^+ \rightarrow Br^- \text{ to } 2HOI \qquad (2)$$

State SSII has higher concentrations of HIO_2, HOBr, and $HBrO_2$ and lower pH compared with SSI. Although lower than in SSI, [HOI] is still higher than $[HBrO_2]$ and [HOBr]. The faster reactions are reactions R3, R11, and R12, which sum to

$$HBrO_2 + I^- \rightarrow Br^- + HIO_2 \qquad (3)$$

Reactions 2 and 3 explain the higher [HOI] in SSI and higher $[HIO_2]$ in SSII.

To understand the oscillations, we examine changes in concentrations for different species and velocities of the model reactions during one cycle of oscillation (Figures 8 and 9). In addition to the graphed concentrations (Figure 8), [IBr] shows oscillations that follow the shape of $[I_2]$ oscillations, but in a lower concentration range (around 1×10^{-11} M). The species $[BrO_2^-]$ and $[HIO_2]$ do not show oscillations and remain at 6×10^{-4} and 1×10^{-4} M, respectively. For simplicity [IBr], $[BrO_2^-]$, and $[HIO_2]$ are not shown.

Starting the cycle from SSII (left, Figures 8 and 9) and increasing time until the vertical line is reached, two separate types of dynamical behavior can be identified: species that decrease in concentration (H^+, $HBrO_2$, HOBr) and species that increase in concentration (I_2, IBr, HOI, I^-, BrO^-). After the vertical line is crossed, the system enters SSI and these trends are

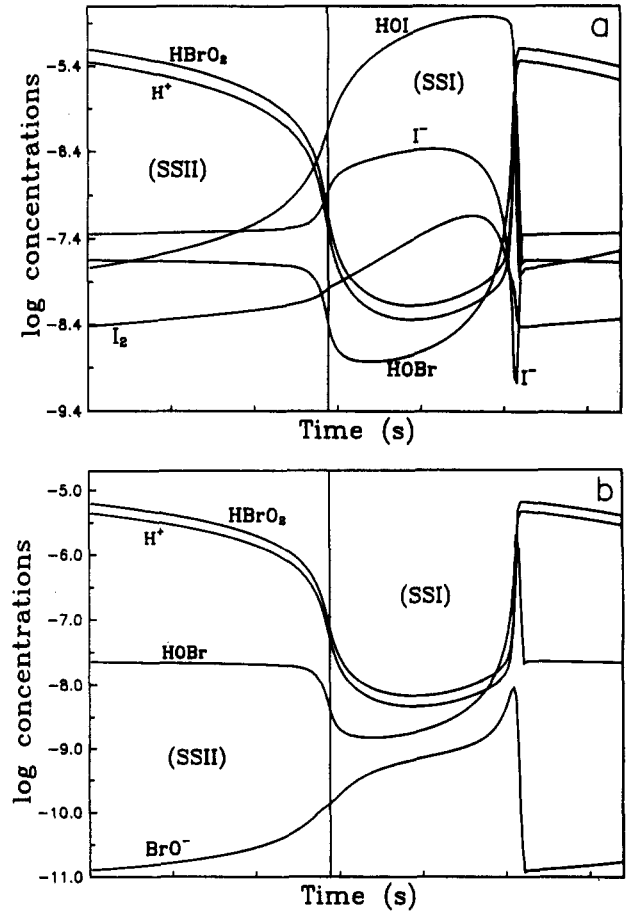

Figure 8. Br(III)–I^-: log concentration–time plots. Initial conditions: $[I^-]_0 = 2 \times 10^{-3}$ M, $[BrO_2^-]_0 = 3.5 \times 10^{-3}$ M, $[H^+]_0 = 1 \times 10^{-4}$ M, $k_0 = 3 \times 10^{-3}\ s^{-1}$. Each division equals 1 s.

reversed, ending in a rapid event characterized by a very substantial decrease in $[I^-]$, whereupon the system enters SSII again (not labeled). This description of oscillation resembles that of the clock behavior found in batch,[3] where the system builds up iodine, which is consumed in a fast event. Explanations given for the batch clock event are a little different, depending on pH (6, 7, or 8).[3] The clock reaction simulation is least accurate at pH 8, where the chemistry is least understood. We believe that this deficiency causes the calculation of shorter periods compared with experiment. In general, oscillatory behavior is more complex than clock behavior, and in this case both pH as well as halogen-containing species oscillate.

Oscillations in pH can be explained by considering the two overall reactions that account for iodine and iodate formation from iodide.

$$4I^- + HBrO_2 + 3H^+ \rightarrow 2I_2 + Br^- + 2H_2O \qquad (4)$$

$$2I^- + 3HBrO_2 \rightarrow 2IO_3^- + 3Br^- + 3H^+ \qquad (5)$$

When the system is under control of reaction 5, it is in SSII (left, Figures 8 and 9) and $[H^+]$ is high. In SSII $HBrO_2$ is in excess over I^-. Iodine and iodide do not accumulate but HOI does. As reaction 2 shows, the accumulation of HOI consumes H^+. This continuous decrease in $[H^+]$ reduces $[HBrO_2]$ by the fast equilibrium R1, and causes the system to switch from SSII to SSI (vertical line, Figures 8 and 9).

In SSI I^- is in excess over $HBrO_2$. The system is under control of reaction 4, which keeps $[H^+]$ low, and I_2 accumulates. At this low $[H^+]$, concentrations of the oxy acids $HBrO_2$ and HOBr are much lower than in SSII, because of the dissociation equilibria R1 and R8. Deficiency of these acids slows almost all reactions

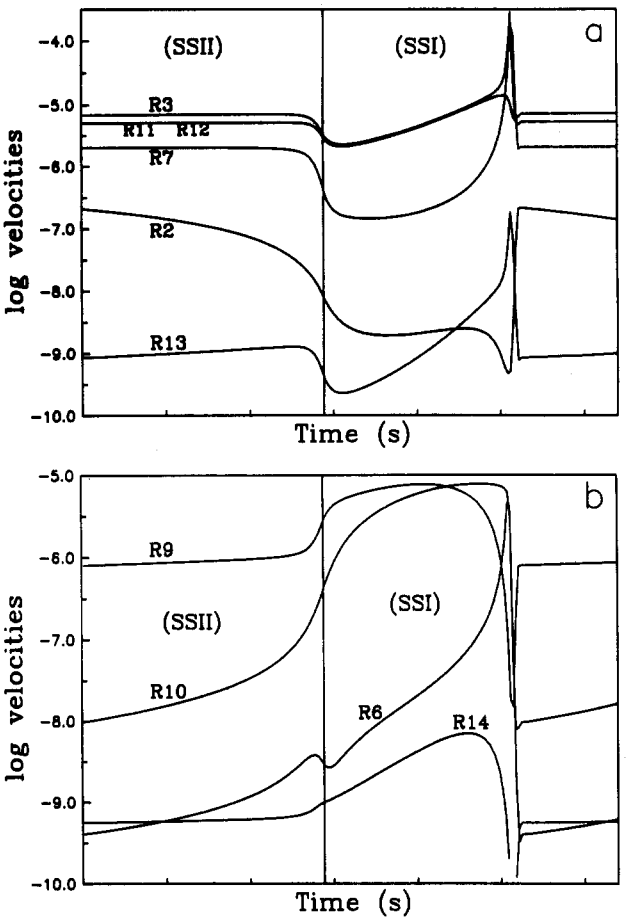

Figure 9. Br(III)–I⁻: velocities of selected reactions in the oscillation state. Initial conditions same as in Figure 8.

and I^-, I_2, and Br(I) (HOBr + BrO^-) increase. The resulting accumulation of Br(I) is the key for switching the system back from SSI to SSII as follows.

In SSI, continuous accumulation of Br(I) brings about an increase of [HOBr]. Velocities of HOBr reactions (especially with iodine) increase, building up HOI in a pathway (R13 + R11) that increases $[H^+]$, as eq 6 shows.

$$HOBr + I_2 + H_2O \rightarrow Br^- + 2HOI + H^+ \qquad (6)$$

Increasing HOI increases the rate of reaction R3, re-forming HOBr and keeping $[HIO_2]$ constant. As can be seen from Figure 9, as the system gets close to the end of SSI (abrupt changes in concentrations and velocities in Figures 8 and 9), the increases in [HOI] and [HOBr] make the set of reactions R3, R11, R12 (Figure 9a) and R9, R10, and R6 (Figure 9b) the fastest reactions. They sum to give eq 7. Therefore, $[H^+]$ increases, which forms

$$HBrO_2\ HOBr + I^- \rightarrow 2Br^- + IO_3^- + 2H^+ \qquad (7)$$

more HOBr and $HBrO_2$ from their anions, resulting in rapid consumption of I^-. The system then switches back to SSII, because $HBrO_2$ is in excess over I^-. Control is again conferred to reaction 5 and a new cycle starts.

Bromine(V)–Iodide. The steady states of our model are similar to those of the CE model (Table V). In agreement with experimental results, SSI shows higher $[I_2]$, which explains this state's brown color. State SSII shows higher values for [IBr], $[HIO_2]$, [HOI], and [HOBr] than SSI. Velocities in SSII are, in general, higher than for SSI, especially the reverse of reaction R11.

Two features characterize our model: relatively high [IBr] throughout (Figure 10a) and the sequential clocklike behavior of individual components. There are species that display minima

TABLE V: Calculated Concentrations and Rates in SSI and SSII at Same Conditions (Bistability Region) for the System Bromine(V)–Iodide[a,b]

	concn (M)			concn (M)	
	SSI	SSII		SSI	SSII
$[BrO_3^-]$	4.5×10^{-3}	3.5×10^{-3}	[HOBr]	9.1×10^{-10}	7.8×10^{-8}
$[I^-]$	3.9×10^{-6}	6.5×10^{-11}	$[Br^-]$	4.2×10^{-4}	2.6×10^{-4}
$[HBrO_2]$	8.3×10^{-9}	4.6×10^{-8}	$[I_2]$	1.2×10^{-3}	7.9×10^{-5}
[HOI]	1.0×10^{-10}	6.2×10^{-7}	[IBr]	3.2×10^{-7}	1.2×10^{-3}
$[HIO_2]$	6.5×10^{-9}	2.0×10^{-4}			

	rate ($M\ s^{-1}$)			rate ($M\ s^{-1}$)	
	SSI	SSII		SSI	SSII
R2	2.4×10^{-8}	2.2×10^{-12}	R12	1.8×10^{-5}	2.5×10^{-8}
R3	5.0×10^{-11}	1.7×10^{-6}	R13	1.1×10^{-5}	6.1×10^{-5}
R4	1.0×10^{-5}	3.6×10^{-5}	R14	3.4×10^{-5}	6.3×10^{-5}
R5	1.5×10^{-13}	4.6×10^{-12}	R15	3.0×10^{-10}	-1.9×10^{-11}
R6	9.1×10^{-14}	4.8×10^{-8}	R16	3.0×10^{-10}	-1.9×10^{-11}
R7	5.9×10^{-12}	1.5×10^{-5}	R17	1.8×10^{-6}	2.3×10^{-11}
R9	5.1×10^{-9}	2.6×10^{-9}	R18	5.5×10^{-9}	2.6×10^{-5}
R10	3.9×10^{-15}	7.3×10^{-7}	R19	3.0×10^{-10}	6.9×10^{-6}
R11	-8.8×10^{-4}	-4.8	R20	8.6×10^{-6}	4.1×10^{-6}

[a] $[I^-]_0 = 2.5 \times 10^{-3}$ M, $[BrO_3^-]_0 = 5 \times 10^{-3}$ M, $[H^+]_0 = 1.5 \times 10^{-4}$ M, $k_0 = 2.5 \times 10^{-2}\ s^{-1}$. [b] Reverse rates are negative.

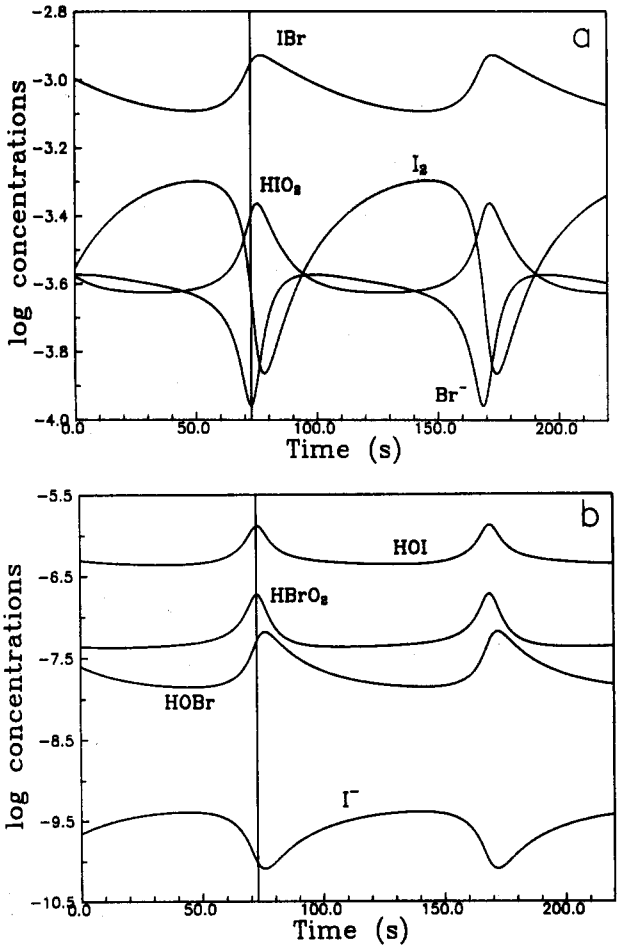

Figure 10. Br(V)–I⁻: log concentration–time plots; higher concentration set (a); lower concentration set (b). Initial conditions: $[I^-]_0 = 2.5 \times 10^{-3}$ M, $[BrO_3^-]_0 = 5 \times 10^{-3}$ M, $[H^+]_0 = 1.5$ M, $k_0 = 3.48 \times 10^{-2}\ s^{-1}$.

in their kinetics curves when the system "clocks" (I_2, I^-, Br^-) and others that display maxima (IBr, HIO_2, HOI, $HBrO_2$, HOBr). In this system, $[BrO_3^-]$ is fairly constant, $\sim 4 \times 10^{-3}$ M; $[I_2OH^-]$ (not shown) follows $[I_2]$ but, at the high acidity of this system, in the range 1×10^{-13} to 1×10^{-14} M.

The key to explaining the behavior of this oscillator is that a simultaneous shortage of Br^- and I^- (Figure 10) causes a buildup

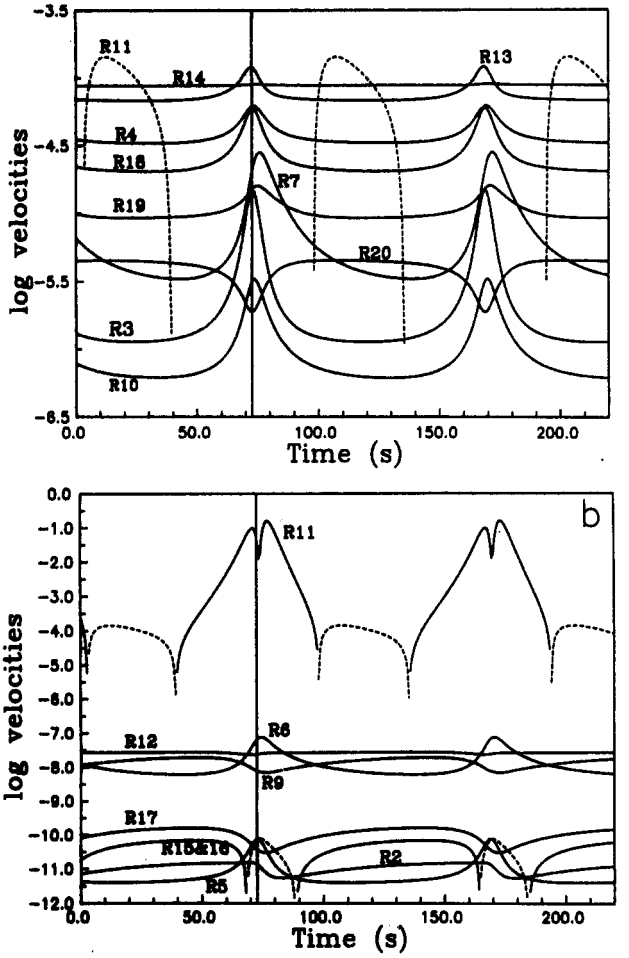

Figure 11. Br(V)–I⁻: log velocities of selected reactions in the oscillatory state. Higher value set (a); lower value set (b). Fixed constraints: $[I^-]_0 = 2.5 \times 10^{-3}$ M, $[BrO_3^-]_0 = 5 \times 10^{-3}$ M, $[H^+]_0 = 1.5$ M, $k_0 = 3.48 \times 10^{-2}$ s^{-1}. Dashed lines indicate reactions running in the reverse direction.

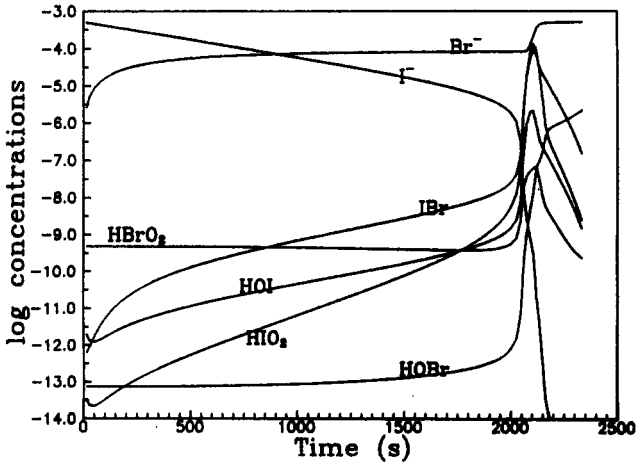

Figure 12. Br(V)–I⁻: log concentration–time plots in batch. Initial conditions: $[I^-]_0 = 5 \times 10^{-4}$ M, $[BrO_3^-]_0 = 5 \times 10^{-3}$ M, $[H^+]_0 = 0.04$ M.

of HOBr, allowing the velocity (Figure 11a) of reaction R13 to increase, thereby consuming I_2 faster than it can be made by reaction R14. As we approach the clock time (vertical line, (Figures 10 and 11)), the two faster reactions are reactions R11 and R13, which sum (eq 6) to form 2 mol of HOI from each I_2. This effect is confirmed by the simultaneous increase of [HOI] and [$HBrO_2$] via reaction R18, which is the faster reaction for the reagent BrO_3^-, always present in excess.

Turning to the batch reaction, we see that the clock event is caused by the shortage of iodide (Figure 12). Reagent [BrO_3^-]

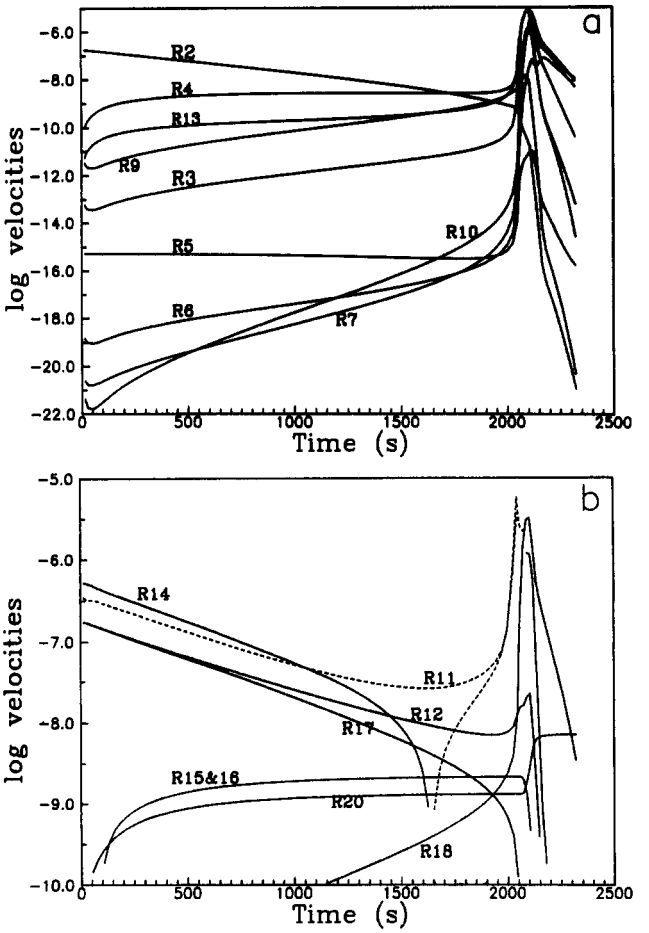

Figure 13. Br(V)–I⁻: log velocities of selected reactions in batch. Initial conditions: same as in Figure 12. Dashed lines indicate reactions running in the reverse direction. Note that reaction R14 changes direction around 1600 s.

is basically constant, its value close to the starting concentration at all times, even at the clock time, because this reagent is in excess (not shown). During the time iodine accumulates, the fastest reactions (Figure 13) are reactions R2, R14, R11, R12, R17, and R4. The first large change caused by the reduction of [I^-] is the inversion of direction of reaction R14 (Figure 13b) at 1600 s, which starts a buildup of IBr instead of producing iodine. The key event, however, is caused by the increase in [HOBr], the fastest reaction of which is with iodide, making more IBr. When [I^-] becomes low enough, HOBr reacts mostly with iodine by reaction R13, which makes more HOI and speeds up reaction R18. As Br^- is the final product for bromine atoms, bromide is always accumulating in this closed system; therefore, the rate of reaction R4 (Figure 13a) accelerates from the increase of $HBrO_2$ made from reaction R18. Putting these reactions together (R13 + R18 + R4) yields an autocatalytic path for HOBr that will rapdily consume iodine and build up IBr.

$$HOBr + I_2 + BrO_3^- + Br^- + 2H^+ \rightarrow IBr + HIO_2 + 2HOBr \quad (8)$$

Conclusions

The oxidations of I^- by Br(III) and Br(V) have a chemistry in common, because they share chemical intermediates in common, such as HOBr, HOI, and HIO_2, but the complexity underlying the dynamics of these systems does not allow easy simplifications. To understand these systems, one must take the full set of differential equations that describes the mechanism, choose from among different conditions, perturb the system in different ways, and follow the response, comparing it with experimental reality for similarities and differences. After carrying out such a

program, we could not identify a smaller set of reactions than those proposed that adequately describes the system in different phases of oscillations, or even adequately describes the batch reaction dynamics of both the bromine(III) and bromine(V) oxidations of iodide ion.

Having a combined mechanism for both systems is a significant improvement in comprehending the nonlinear dynamics of these halogen-based chemical oscillators. Additional experimental and modeling studies are needed to combine other halogen oscillators under a single set of rate constants that do not need be changed from one system to another, except for obligatory corrections for changes of temperature and ionic strength.

Acknowledgment. This work was supported by Research Grant CHE-9023294 and U.S.–Hungarian Cooperative Grant INT-8921816 from the National Science Foundation and by Conselho Nacional de Desenvolvimento Científico e Tecnológico-CNPq (Proc. 202081/90-7).

Registry No. The following Registry numbers were supplied by the author. I^-, 20461-54-5; $HBrO_2$, 37691-27-3; BrO_2^-, 7486-26-2; BrO_3^-, 15541-45-4.

References and Notes

(1) Systematic Design of Chemical Oscillators. 86. For part 85, see: Rábai, G.; Wang, R. T.; Kustin, K. *Int. J. Chem. Kinet.*, in press.
(2) Orbán, M.; Epstein, I. R. *J. Am. Chem. Soc.* **1992**, *114*, 1252.
(3) Faria, R. B.; Epstein, I. R.; Kustin, K. *J. Am. Chem. Soc.* **1992**, *114*, 7164.
(4) Faria, R. B.; Epstein, I. R.; Kustin, K. *J. Phys. Chem.* **1992**, *96*, 6861.
(5) Simoyi, R. H.; Masvikeni, P.; Sikosana, A. *J. Phys. Chem.* **1986**, *90*, 4126.
(6) Alamgir, M.; De Kepper, P.; Orbán, M.; Epstein, I. R. *J. Am. Chem. Soc.* **1983**, *105*, 2641.
(7) Citri, O.; Epstein, I. R. *J. Am. Chem. Soc.* **1986**, *108*, 357.
(8) Kaps, P.; Rentrop, P. *Numer. Math.* **1979**, *33*, 55.
(9) Sweeton, F. H.; Mesmer, R. E.; Baes, Jr., C. F. *J. Solution Chem.* **1974**, 191.
(10) Györgyi, L.; Rempe, S. L.; Field, R. J. *J. Phys. Chem.* **1991**, *95*, 3159.
(11) Györgyi, L.; Turányi, T.; Field, R. J. *J. Phys. Chem.* **1990**, *94*, 7162.
(12) Noszticzius, Z.; Noszticzius, E.; Schelly, Z. A. *J. Phys. Chem.* **1983**, *87*, 510.
(13) Ariese, F.; Ungvárai-Nagy, Z. *J. Phys. Chem.* **1986**, *90*, 1.
(14) Citri, O.; Epstein, I. R. *J. Phys. Chem.* **1988**, *92*, 1865.
(15) Troy, R. C.; Kelley, M. D.; Nagy, J. C.; Margerum, D. W. *Inorg. Chem.* **1991**, *30*, 4838.
(16) Bard, A. J., Parsons, R., Jordan, J., Eds. *Standard Potentials in Aqueous Solutions*; Marcel Dekker: New York, 1985.
(17) Capone, S.; De Robertis, A.; De Stefano, C.; Sammartano, S.; Scarcella, R. *Talanta* **1987**, *34*, 593.
(18) Meites, L., Ed. *Handbook of Analytical Chemistry*; McGraw-Hill: New York, 1963; p 1.8.
(19) Kshirsagar, G.; Field, R. J. *J. Chem. Phys.* **1988**, *92*, 7074.
(20) Noszticzius, Z.; Gáspár, V.; Försterling, H.-D. *J. Am. Chem. Soc.* **1985**, *107*, 2314.
(21) Eigen, M.; Kustin, K. *J. Am. Chem. Soc.* **1962**, *84*, 1355.
(22) Atkins, P. W., *Physical Chemistry*, 4th ed.; W. H. Freeman: New York, 1990; p 221.
(23) Ermentrout, B. *Phaseplane, Version 3.0*; Brooks/Cole: Pacific Grove, CA, 1990.